Available online at www.sciencedirect.com
SCIENCE DIRECT
Journal of Magnetic Resonance 181 (2006) 342–349
JMR Journal of Magnetic Resonance
www.elsevier.com/locate/jmr

Communication

Fast and quiet MRI using a swept radiofrequency

Djaudat Idiyatullin, Curt Corum, Jang-Yeon Park, Michael Garwood *

Center for Magnetic Resonance Research, Cancer Center and Department of Radiology, University of Minnesota Medical School, 2021 6th St. SE, Minneapolis, MN 55455, USA

Received 4 February 2006; revised 25 April 2006
Available online 19 June 2006

Abstract

A novel fast and quiet method of magnetic resonance imaging (MRI) is introduced which creates new opportunities for imaging in medicine and materials science. The method is called SWIFT, sweep imaging with Fourier transformation. In SWIFT, time-domain signals are acquired in a time-shared manner during a swept radiofrequency excitation of the nuclear spins. With negligible time between excitation and signal acquisition, new possibilities exist for imaging objects consisting of spins with extremely fast transverse relaxation rates, such as macromolecules, semi-solids, and quadrupolar nuclei. The field gradient used for spatial-encoding is not pulsed on and off, but rather is stepped in orientation in an incremental manner, which results in low acoustic noise. This unique acquisition method is expected to be relatively insensitive to sample motion, which is important for imaging live objects. Additionally, the frequency-swept excitation distributes the signal energy in time and thus dynamic range requirements for proper signal digitization are reduced compared with conventional MRI. For demonstration, images of a plastic object and cortical bone are shown.

Keywords: MRI; Sweep excitation; Radial imaging; Adiabatic pulses; Correlation spectroscopy

1. Introduction

NMR signal is observed following one of three basic types of radiofrequency (RF) excitation: sequential, simultaneous, and random. Accordingly, three different types of NMR techniques have been developed: continuous wave (CW) [1,2], pulsed [3–5], and stochastic [6,7]. Historically, the first high resolution NMR spectra of liquid samples were acquired using the CW technique. NMR spectroscopy using the CW technique became an important tool in the field of chemistry until the early 1970's. Then, shortly after realizing the efficiency of pulsed Fourier transform (FT) spectroscopy [8], pulsed FT supplanted CW as the main spectroscopic technique. Nowadays, pulsed FT spectroscopy continues to dominate the field, while the CW and stochastic NMR techniques are mainly used only for niche applications.

Magnetic resonance imaging (MRI) has additional technical requirements over high-resolution NMR spectroscopy of liquids. Because the object to be imaged is usually much larger than a sample tube, inevitably the static and RF fields used in MRI are more inhomogeneous than those used in high resolution NMR. Furthermore, MRI requires high power RF amplifiers to attain a sufficiently intense RF field to excite all spins simultaneously. In a search for ways to circumvent such difficulties, some researchers have reconsidered old, almost forgotten NMR techniques. For this reason, the "sleeping beauty" [9], stochastic NMR, was reawakened [10] and found to have remarkable features; most notably, the peak RF power required for spin excitation is at least two orders of magnitude lower than that required by conventional pulsed schemes. Very recently, a CW MRI system using low peak RF power has also been developed and applied to study a variety of heterogeneous materials exhibiting extremely fast spin–spin relaxation [11]. Another example is the extensive application in modern MRI of adiabatic sweep pulses, which evolved from the traditional

* Corresponding author. Fax: +1 612 626 2004.
E-mail address: gar@cmrr.umn.edu (M. Garwood).

1090-7807/$ - see front matter © 2006 Elsevier Inc. All rights reserved.
doi:10.1016/j.jmr.2006.05.014

CW technique. An advantage of the adiabatic sweep pulse is its ability to accomplish uniform rotation over a broad band of resonance frequencies [12].

This article presents a new MRI method that can be considered as a combination of all three basic NMR techniques. As in CW NMR, this new method uses swept RF excitation, but the sweep rate far exceeds the CW sweep rate even during a rapid-scan [13,14]. Unlike the CW method in which the signal is acquired in the frequency domain, here the signal is treated as a function of time, as in the pulsed FT method. Finally, the method uses correlation, identical to that used in stochastic NMR, to extract the signal arising from the spin system. This novel method is dubbed SWIFT, for sweep imaging with Fourier transformation. The concept of using swept RF excitation instead of a monochromatic RF pulse or stochastic excitation and then reconstructing the NMR spectrum using the correlation method, was mentioned more than three decades ago [13], but was never put into practice.

The main advantage of SWIFT originates in its nearly simultaneous excitation and acquisition scheme. In conventional MRI, excitation and acquisition events are separated by the length of time known as the echo time (T_E), which is typically >1 ms. This length of time is too long to allow detection of slowly tumbling nuclei with short spin–spin relaxation time (T_2). By comparison, SWIFT allows $T_E \approx 0$, because signal acquisition can begin within a few microseconds after excitation. Thus, SWIFT is a powerful tool for imaging objects having a broad distribution of relaxation times, including very short T_2 values. In particular, the method is expected to find extensive application for imaging and spectroscopy of semi-solid objects such as bone, macromolecules, and quadrupolar nuclei such as sodium-23 [15], potassium-39 [16], and boron-11 [17]. Here, a description of the new technique is provided, and proof-of-principle is shown by simulated and experimental data.

2. Sweeping technique

The simplest realization of the SWIFT method is presented in Fig. 1a. The scheme employs a sequence of RF pulses, each having a duration T_p typically in the millisecond range. In the present implementation, the RF pulse is one of the family of adiabatic hyperbolic secant (HSn) pulses [12,18,19] which utilizes both amplitude and frequency modulation. The amplitude of the pulse is denoted by the variable $\omega_1(t)$ $(= \gamma B_1(t)$, where γ is the gyromagnetic ratio and $B_1(t)$ is the time-dependent amplitude of the RF field), and the time-dependent frequency of the pulse is denoted by $\omega_{RF}(t)$, both in units of rad/s. The pulse is divided into N segments, each having RF power on for duration τ_p, following a delay with RF power off. Data sampling is performed at time τ_a after the pulse segment. The dwell time of data sampling is $dw = T_p/N$, and the maximum excitation bandwidth (B_w) according to the Nyquist theorem is equal to the acquisition spectral width (sw):

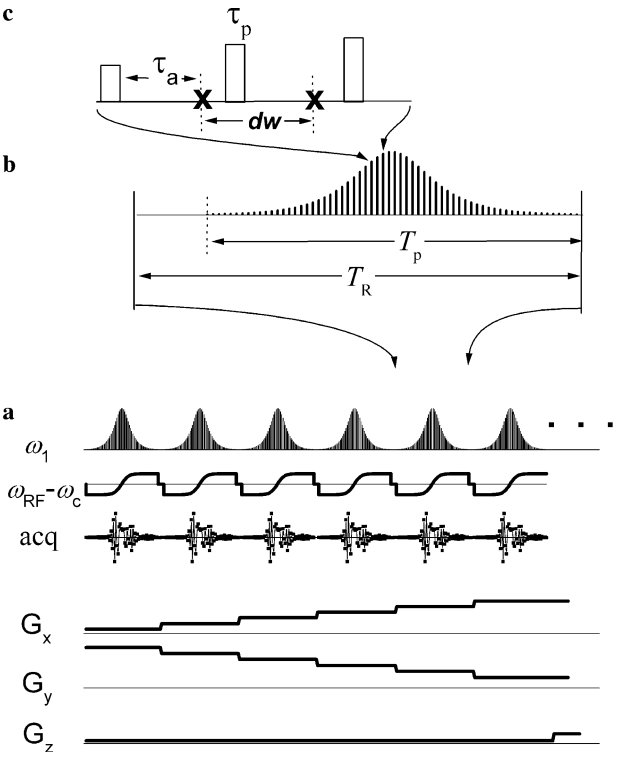

Fig. 1. The SWIFT pulse sequence scheme (a) and detailed presentation of the repeated part of the sequence (b) and magnified presentation of the pulse segments (c). A number of dummy scans with changing view orientation are needed to obtain a steady-state before starting the actual acquisition.

$$B_w = sw = 2\pi \frac{N}{T_p}. \tag{1}$$

This type of time-shared excitation and signal acquisition is played out in the presence of an applied magnetic field gradient $\mathbf{G} = (G_x\hat{i} + G_y\hat{j} + G_z\hat{k})$ used to impart on the spins a spatially dependent Larmor frequency $\omega(\mathbf{r}) = \gamma(G\mathbf{r} + B_0)$, where $\mathbf{r}$ is the coordinate vector and B_0 is the static magnetic field. The minimum temporal spacing of pulses, or repetition time (T_R), is simply T_p plus the amount of time (t_G) needed to make an incremental change in the orientation of $\mathbf{G}$. After acquiring a full set of frequency-encoded projections, 3D images can be reconstructed using a 3D back-projection algorithm [20] or gridding [21]. The minimum acquisition time required to obtain each projection is

$$A_t = t_G + 2\pi N/sw. \tag{2}$$

For example, with acquisition parameters that standard MRI scanners can readily achieve, $sw/2\pi = 100$ kHz and $t_G = 0.3$ ms, a 3D image with matrix size $= 128 \times 128 \times 128$ can be acquired in less than 30 s. A further ~30% time reduction is possible without affecting image quality using an equidistant projection sampling method [20].

In the SWIFT sequence, unwanted spin and stimulated echoes are effectively spoiled during the period t_G when the readout gradient is set to a new orientation. In addition, the frequency-swept pulses sequentially excite isochromats, and as a result, the phase of the magnetization

varies in a quadratic manner along the readout direction (i.e., traditional echoes are not created [25]).

Computer simulations based on the classical Bloch equations can help to reveal the behavior of spins during the application of such amplitude- and frequency-modulated pulses. Fig. 2 shows the oscillatory motion of the magnetization components of a given isochromat having frequency ω. In the figure, $M_x^{\mathrm{PM}}(t)$ presents the x-axis component of the transverse magnetization vector of this isochromat in a reference frame known as the phase-modulated (PM) frame [12], which rotates around the static magnetic field direction (z) with an angular velocity ω_c equal to the center frequency in the sweep range. $M_x^{\mathrm{FM}}(t)$ is the x-axis component in a frequency-modulated (FM) frame, which rotates synchronously with the (time-dependent) pulse frequency $\omega_{\mathrm{RF}}(t)$ [12]. The figure also shows the absolute value of the transverse magnetization, $M_{xy}(t)\left(=\sqrt{M_x^2(t)+M_y^2(t)}\right)$. Similar oscillatory behavior was observed in the early days of NMR [22], and is known to arise in the *rapid passage*, *linear region*, which satisfies the conditions [23]

$$aT_2^2 >> 1 \tag{3a}$$

and

$$a/\omega_1^2 >> 1, \tag{3b}$$

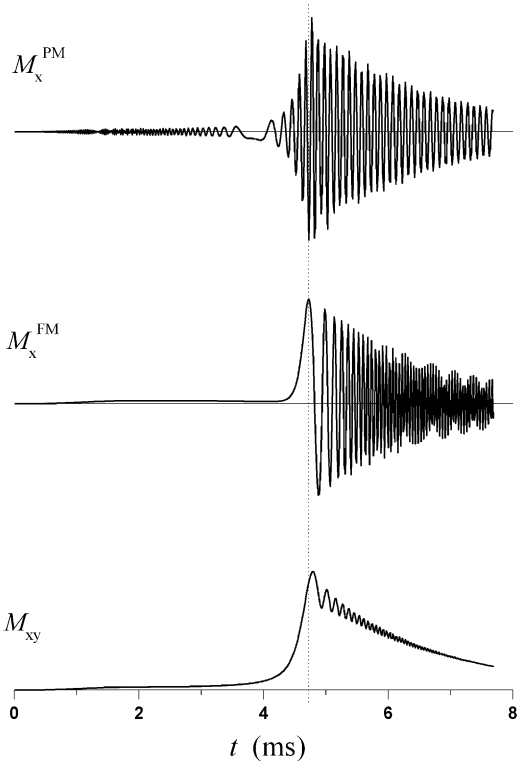

Fig. 2. Results of simulations using the HS8 pulse for frequency-swept excitation. Data shown include the M_x component in the phase-modulated (M_x^{PM}) and frequency-modulated rotating frames (M_x^{FM}), and the magnitude (M_{xy}), of a single isochromat.

where a is the sweep rate; in our case $a \approx B_w/2\pi T_p$. It is important to note the difference between the *rapid passage*, *linear region* and the *rapid passage*, *adiabatic region*, wherein the latter condition is $a/\omega_1^2 << 1$. Accordingly, the transition from the adiabatic to the linear region requires reducing the RF amplitude or increasing the sweep rate, while other pulse parameters remain constant. In this way, an adiabatic passage pulse, such as a HSn pulse, can be used in the *rapid passage*, *linear region* to rotate the magnetization by an angle $\leqslant 90°$, as needed for excitation in SWIFT. Below, all presented simulated and experimental data were generated using excitation in the *rapid passage*, *linear region*.

In the first approximation, the RF field excites each isochromat *instantaneously* when its resonance frequency is attained in the frequency sweep [24,25]. In Fig. 2, the time of resonance for this particular isochromat is denoted by the vertical dotted line. Although the instantaneous approximation is quite good, it can be seen that a small amount of transverse magnetization is produced before resonance is observed. Note that the oscillations before resonance are completely absent in the FM frame ($M_x^{\mathrm{FM}}(t)$). This means that the oscillations are a consequence of the frequency modulation $\omega_{\mathrm{RF}}(t)$, and thus, are a reflection of the pulse, rather than free precession. From these simulations, it is apparent that the magnetization follows the effective RF field vector until the time of resonance, when the isochromat is released from the "hug" of the RF pulse and decays due to transverse relaxation (in this case, $T_2 = 2$ ms). The isochromat then evolves, but not without a residual effect from $\omega_{\mathrm{RF}}(t)$, as is apparent from the oscillations in $M_{xy}(t)$.

To obtain an image of an object using SWIFT, additional steps are needed to remove the $\omega_{\mathrm{RF}}(t)$ oscillations described above, since simple FT of the time-domain signals would yield a spectrum (in this case, a projection of the object) that is contaminated by the frequency components of $\omega_{\mathrm{RF}}(t)$. In the SWIFT technique, processing is done using a cross-correlation method identical to that used to recover phase information in stochastic NMR spectroscopy [6,7]. Accordingly, the spin system response is treated as a linear system; a concept that is often used in NMR. The response $r(t)$ of the linear system to the input function $x(t)$ is the convolution process given by

$$r(t) = h(t) \otimes x(t). \tag{4}$$

According to the standard nomenclature used in NMR, the unit impulse response $h(t)$ is the free induction decay (FID) and the unit frequency response function is the spectrum $H(\omega)$, and these functions are related to one another by direct FT [8,26]. According to Fourier theory, the convolution in the time domain is a complex multiplication in the frequency co-domain

$$\mathbf{F}\{r(t)\} = R(\omega) = H(\omega)X(\omega), \tag{5}$$

where $X(\omega)$ is the FT of the input function $x(t)$, which in our case is

$$x(t) = \omega_1(t)\exp\{-\mathrm{i}(\omega_{\mathrm{RF}}(t) - \omega_c)t\}. \quad (6)$$

The spectrum of the system can be retrieved by using correlation, which is straightforward to perform in the frequency domain with complex conjugate multiplication by the pulse function [27]

$$H(\omega) = \frac{R(\omega)X^*(\omega)}{|X(\omega)|^2}, \quad (7)$$

where $|X(\omega)|$ is the modulus of $X(\omega)$. The spectral profile of the HS*n* pulses is highly uniform within the bandwidth [12], and as a result, $|X(\omega)|$ is essentially constant across the spectrum.

To illustrate the correlation method, Fig. 3 presents simulated results in the frequency domain for the case of a 1D object with isochromats distributed according to a step function $M_0(\omega)$. Fig. 3 displays the real components of the response $R_x(\omega)$ and pulse $X_x(\omega)$, and the real and imaginary parts of the correlated spectrum, $H_x(\omega)$ and $H_y(\omega)$. It is apparent that $R_x(\omega)$ has scrambled phase and contains contaminant signals arising from the $\omega_{\mathrm{RF}}(t)$ oscillations, which contain all frequencies in the spectral window. The correlated absorption spectrum of the system $H_x(\omega)$ was obtained from Eq. (7) and by applying a first order phase correction. It can be seen that $H_x(\omega)$ is almost an exact replica of the spin density profile $M_0(\omega)$. All contaminant signals from the oscillations are present only in the imaginary component of the spectrum $H_y(\omega)$.

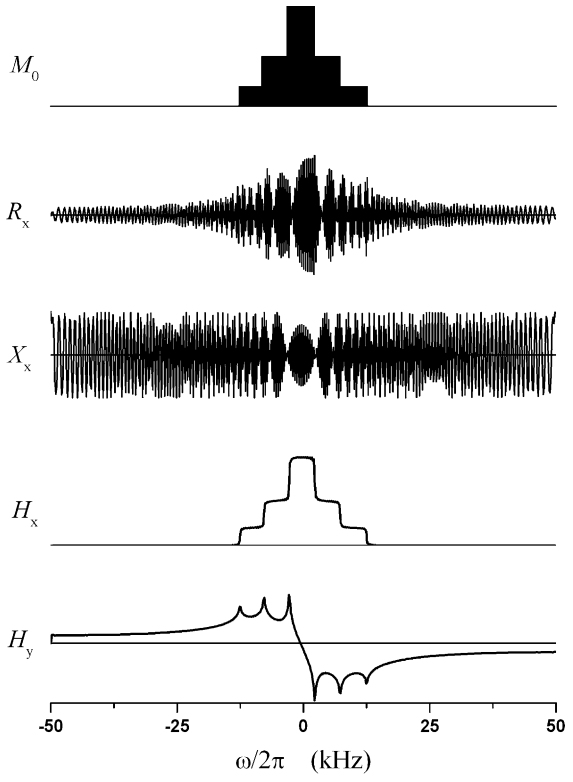

Fig. 3. Real parts of the response (R_x) and the RF pulse spectrum (X_x), and the real (H_x) and imaginary (H_y) parts of the system spectrum. These simulation results shown are in the frequency domain, and were obtained using an array of 100 isochromats spaced 250 Hz apart, with amplitudes weighted according to a step function, $M_0(\omega)$. Frequency-swept excitation was produced with the HS8 pulse using $\tau_p = dw$ and $sw/2\pi = 100$ kHz.

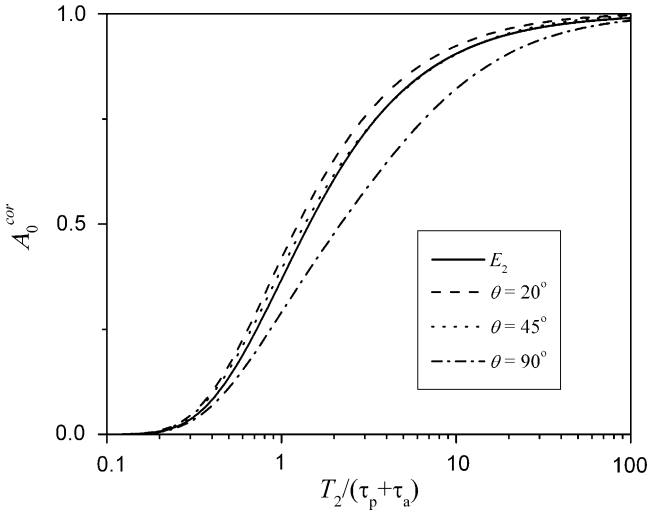

Fig. 4. Simulated excitation performance of the HS1 pulse in the intermediate passage region. The normalized amplitude of the excited magnetization A_0^{cor} is shown to depend on the flip angle θ and the normalized T_2. The $\omega_1(t)$ function was scaled to produce 20°, 45°, and 90° flip angles in the absence of relaxation ($T_2 \Rightarrow \infty$). $E_2 = \exp(-(\tau_p + \tau_a)/T_2)$ (details in text).

It is worth emphasizing that the SWIFT sequence has less stringent constraints than indicated by Eqs. (3a) and (3b). First of all, because the pulse is segmented, the average value of $\omega_1(t)$ scales inversely with τ_p/dw. Second, according to simulation and experimental data, the correlation method works well up to a rotation angle near 90° before significantly violating the linearity condition of Eq. (3b). On the other hand, the SWIFT technique is not restricted to the *rapid passage region* by Eq. (3a), but instead can be used in the *intermediate passage*, *linear region* [23], with the consequences of sacrificing signal-to-noise ratio (S/N) and resolution. To illustrate this point, Fig. 4 presents the excitation performance of the HS1 pulse in the *intermediate passage region*. The simulated parameter A_0^{cor} is the normalized amplitude of the FID obtained by inverse FT of the correlated spectra. A_0^{cor} is normalized to be equal to 1 for $T_2 \Rightarrow \infty$. A_0^{cor} is plotted against $T_2/(\tau_p + \tau_a)$ using different excitation flip angle θ (θ calculated for $T_2 \Rightarrow \infty$). The function $E_2 = \exp(-(\tau_p + \tau_a)/T_2)$ (solid line) well describes the dependencies. From this simulation, it can be seen that the limit of the T_2 sensitivity of the SWIFT sequence is $T_2 \geqslant \tau_p + \tau_a \sim dw$.

3. Comparison with other excitation methods

3.1. Pulsed FT NMR

In the pulsed FT technique, the excitation pulse is generally assumed to be short (a delta function), so that the FT of this input function can be considered approximately equal to unity, and thus, the system spectrum ($H(\omega)$) can be obtained directly via FT of the impulse response

($h(t)$). In MRI, the RF pulse can approach a delta function only by restricting the flip angle to $\ll 90°$. As the pulse length increases, the pulsed FT spectrum suffers from increasing phase and baseline distortions. Although these artifacts can be avoided by replacing the FID with an echo acquisition, the finite T_E used to form an echo leads to reduced sensitivity to fast relaxing spins and increased susceptibility to motion and flow artifacts.

Theoretically achievable S/N per unit time for the SWIFT technique might be compared with pulsed FT for optimal conditions and employing a matched filter function as it was done for the rapid-scan FT technique [14,28]. Analogously the ratio of the sensitivities of the pulsed FT to the SWIFT experiment performed in the same total time and with the same resolution is

$$\frac{(S/N)_p}{(S/N)_{SWIFT}} = \left[\frac{T_R^{SWIFT}(1-E_1^p)(1+E_1^{SWIFT})}{T_R^p(1+E_1^p)(1-E_1^{SWIFT})}\right]^{1/2}, \quad (8)$$

where $E_1^i = \exp(-T_R^i/T_1)$ is the recovery term and T_R^i is repetition time of excitation pulses. The ideal pulsed FT experiment has repetition time exactly equal to the acquisition time, which must exceed the transverse relaxation time to avoid truncation effects, and usually the setting is $T_R^p \approx 3T_2^*$, where T_2^* is the effective relaxation time including relaxation and static dephasing effects. In the SWIFT experiment, the acquisition time must be two times longer, $T_R^{SWIFT} = 2T_R^p$, to ensure that the last isochromat excited by the pulse is measured for a period $\geqslant 3T_2^*$. Therefore, according to Eq. (8), for $T_1 \gg T_R^i$ (i.e., fast MRI acquisition), $\frac{(S/N)_p}{(S/N)_{SWIFT}} \sim 1$. Even when T_R^p is on the order of T_1, the sensitivity of the pulsed FT experiment exceeds that of the SWIFT experiment by only about 10%.

Certain pulsed FT techniques [29,30] appear at first glance to be closely related to the SWIFT method. These techniques use a short monochromatic RF pulse for excitation, followed immediately by signal acquisition, all performed in the presence of a field gradient. Although these fast imaging sequences, similar to the SWIFT sequence, have minimal demands on gradient hardware performance, they are severely limited by the length of the pulse. To achieve broadband excitation with limited ω_1 amplitude, a small flip angle is employed, which results in low S/N. The SWIFT technique does not suffer this limitation because the excitation bandwidth is not constrained by the amplitude of ω_1. Another technique known as the ultra-short TE (UTE) sequence [31,32] was also developed to image fast relaxing spins using FID acquisition. The UTE sequence employs a self-refocused excitation pulse, followed immediately by a pulsed-on gradient and signal acquisition. The minimum duration needed to execute the excitation pulse and gradient switching are limited by the available RF amplitude and the gradient slew rate, respectively. Due to these technical limitations, the UTE sequence appears to be less effective in capturing signals from fast relaxing spin, as compared with SWIFT.

3.2. CW and rapid-scan FT NMR

The main advantage of the CW method over the pulsed MRI technique is its low RF power requirement. However, due to the slow rate of acquisition, CW MRI is time consuming and thus impractical for *in vivo* applications [11]. Sensitivity enhancement of the CW method was attained with the rapid-scan FT technique [13,14], a close relative to the frequency-swept NMR method introduced here. In comparison with SWIFT, the rapid-scan FT technique possesses certain disadvantages inherent to CW NMR. For example, to avoid non-uniform weighting of the spectrum, the excitation frequency must be swept linearly (chirp pulse), which excludes the use of tailored frequency sweeps (e.g., adiabatic rapid passage pulses such as the HS*n* pulse) and the experimental advantages they can provide.

The distinction between the rapid-scan FT and SWIFT techniques can be further exemplified with the aid of Fig. 2. In the SWIFT technique, the receiver is set to a constant frequency and thus the acquired signal behaves as M_x^{PM} in Fig. 2 with the abscissa representing time (t). Following the excitation time (dotted line), the ensuing evolution resembles a FID. To obtain the spectrum, correlation is used to remove the influence of the $\omega_{RF}(t)$ function and to unscramble the phases of different isochromats having different excitation times. In the rapid-scan FT technique, the detector frequency is synchronous with the time-dependent transmitter frequency, and thus, the acquired signal appears as presented in FM frame (M_x^{FM} in Fig. 2), but with the abscissa representing spectral frequency and the dotted line corresponding to the resonant frequency of the isochromat (ω). In this case, correlation must be used to restore the undistorted absorption line by removing the "ringing" that persists following passage through resonance. The remarkable property that the response can be treated in either the time or frequency domain is a consequence of the fact that the sweeping itself is a function of both time and frequency. In accordance with the Nyquist theorem, sampling in the frequency versus time domain places an upper and lower limit on the sweep rate used in the rapid-scan FT and SWIFT technique, respectively. The lack of an upper limit on the sweep rate is the feature of SWIFT giving its tremendous advantage for MRI.

3.3. Stochastic NMR

Nowadays, stochastic NMR is generally considered to be an exotic technique, even though many years ago it was shown theoretically to offer the same sensitivity as the pulsed FT technique [6]. The advantages of stochastic NMR were overshadowed by the rapid and intensive development of pulsed FT. The main limitation in stochastic NMR is the need to create truly random excitation in order to avoid systematic noise artifacts. This problem can be circumvented by using colored noise with well known excitation spectra, together with a small flip angle (<1°) so the spin system remains in the linear region [10,33]. Although

this approach has been shown to be feasible, its practical utility is limited by the low acquired signal amplitude [34].

In principle, the SWIFT technique, using the same "time shared" acquisition, can be considered to be a branch of stochastic NMR using colored noise excitation. Fortunately, the spin response to the swept RF excitation in SWIFT behaves effectively as a linear system for flip angles up to 90°. Hence, the SWIFT method affords high S/N without observable image artifacts from violating the linearity condition.

4. Image contrast

In the implementation of SWIFT, the magnetic field variation created by the applied gradient **G** can readily exceed other potential contributions (e.g., magnetic susceptibility differences and an inhomogeneous B_0), so their effects are not perceivable in images. SWIFT images are also essentially unaffected by transverse relaxation, provided $T_2 > 10dw$ (see Fig. 4). Under these conditions, the signal intensity depends only on T_1 and spin density (M_0) as [8,28]

$$S = M_0 \frac{1 - E_1^{\mathrm{SWIFT}}}{1 - E_1^{\mathrm{SWIFT}} \cos(\theta)} \sin(\theta). \tag{9}$$

For fixed T_R, the maximum signal intensity is attained with optimum flip angle θ_{opt} which satisfies the equation

$$\cos(\theta_{\mathrm{opt}}) = E_1^{\mathrm{SWIFT}}. \tag{10}$$

T_1 contrast can be evaluated from the derivative of the signal, $\frac{\mathrm{d}S}{\mathrm{d}(1/T_1)}$. For fixed T_R, this derivative has a maximum at $\theta \approx 1.7\theta_{\mathrm{opt}}$. The best compromise between sensitivity and contrast will thus occur in the range $\theta_{\mathrm{opt}} < \theta < 1.7\theta_{\mathrm{opt}}$, where θ_{opt} corresponds to a spin of interest which has the smallest T_1 value. For the case of $\theta \ll \theta_{\mathrm{opt}}$, T_1-weighting becomes negligible, and image contrast is dictated mainly by spin density variations.

5. Experiments

Although many new applications are anticipated for this novel MRI technique, here the utility of SWIFT is demonstrated for imaging spins with extremely short T_2 values (Figs. 5 and 6). The first test object is thermoplastic, which is invisible by conventional MRI because the T_2 value is extremely short (~0.3 ms). As can be seen from Fig. 5, SWIFT produced a highly resolved 3D image of the object. It is worth noting that these images were obtained using a standard MRI scanner (4.7 T) which is not equipped with special software or hardware (e.g., solid state accessory). SWIFT images of *ex vivo* bovine tibia were also acquired to demonstrate the technique's sensitivity to short T_2 spins (Fig. 6). This SWIFT image is also compared to an image acquired using the shortest T_E value (1.6 ms) that could be attained with a standard gradient-echo sequence. The cortical compact bone, which has $T_2 = 0.4$ ms [32], is not

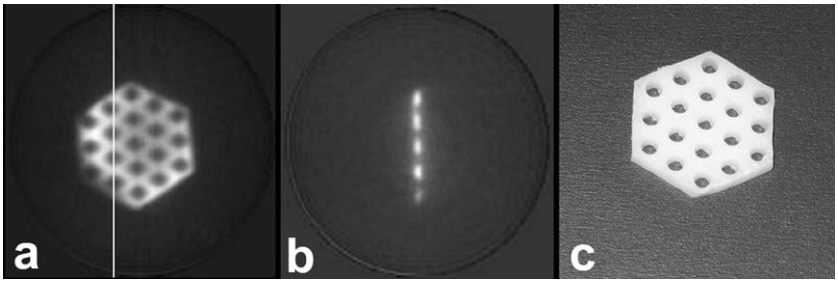

Fig. 5. Selected slices from a 3D image of a thermoplastic object (a and b) having $T_2 \sim 0.3$ ms, and a photograph of the object (c). This sample was used to test the sensitivity of the SWIFT technique to short T_2 spins. The image was acquired using the HS1 pulse, matrix size = $128 \times 128 \times 128$, field-of-view = $50 \times 50 \times 50$ mm^3, $sw/2\pi = 100$ kHz, $T_R = 7.25$ ms, $\theta \approx 30°$, and no signal averaging.

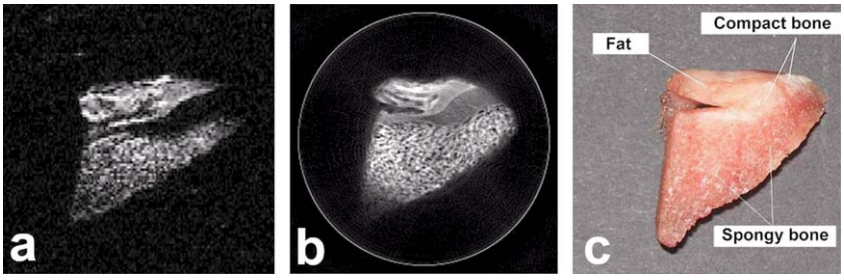

Fig. 6. Conventional 2D gradient echo image (a) and a representative slice of a 3D SWIFT image (b) of a specimen of bovine tibia, and its photograph (c). The gradient echo image was acquired using matrix size = 128×128, $T_R = 50$ ms, slice thickness = 2.25 mm, field-of-view = 30×30 mm^2, and $T_E = 1.6$ ms. The 3D SWIFT image was acquired using the HS1 pulse, matrix size = $256 \times 128 \times 128$, $T_R = 12.56$ ms, field-of-view = $30 \times 30 \times 30$ mm^3. Both acquisitions were performed using $sw/2\pi = 100$ kHz, $\theta \approx 30°$, and no signal averaging.

visible in the gradient-echo image (Fig. 6a), but is easily recognizable in the SWIFT image (Fig. 6b). These early SWIFT images were reconstructed using a standard 3D back-projection algorithm for Figs. 5a and b and gridding for Fig. 6b, with no additional processing (e.g., filtering) to remove subtle image intensity ripples and other minor artifacts.

6. Conclusions

In conclusion, the SWIFT technique has many novel and beneficial properties for MRI:

(a) Fast. The method avoids not only delays associated with refocusing pulses or gradient inversion, but also time for an excitation pulse, which is combined with the acquisition period. Of course, like all fast imaging sequences, SWIFT is limited by existing imaging system hardware and chosen compromise between acquisition speed, spatial resolution and S/N.

(b) Sensitive to short T_2. The method is sensitive to all excited spins having spin–spin relaxation time larger than the reciprocal value of the spectral width, $T_2 > 2\pi/sw$.

(c) Reduced motion artifacts. Because the SWIFT method has no "echo time" it is expected to be less sensitive to motion and flow artifacts than conventional MRI methods. As compared with other fast sequences, SWIFT loses much less signal due to either diffusion in the presence of a gradient or uncompensated motion.

(d) Reduced signal dynamic range. Because different frequencies are excited sequentially the resulting signal is distributed in time, leading to a decreased amplitude of the acquired signal. This allows more effective utilization of the dynamic range of the digitizer.

(e) Quiet. Last, but not the least, the SWIFT method uses a small step when changing gradients between projections, and the fast gradient switching that creates loud noise can be avoided. This property is very important for MRI scanning of the patients having ligyrophobia.

SWIFT can also be operated in a rapid updated mode to reach high temporal resolution in dynamic studies [30]. This pseudo-temporal resolution is possible because projection reconstruction, unlike Fourier imaging, samples the center of k-space with every acquisition.

It remains a historical mystery why the benefits of this swept RF technique were not recognized in the 1970's at the same time as the rapid-scan FT and stochastic NMR techniques were developed. By having the advantages of time-domain methods, the swept RF approach introduced here might eventually compete for some NMR applications currently dominated by pulsed FT techniques. The approach used in the SWIFT technique creates new opportunities for MRI applications in medicine, industry and materials science and represents a valuable addition to the battery of MRI techniques already existing.

Acknowledgments

This research was supported by NIH Grants RR008079 and CA92004. The authors thank Dr. Ivan Tkac for helping with reconstruction software implementation and Dr. Jutta Ellermann for assistance in conducting the experiments.

References

[1] E.M. Purcell, H.C. Torrey, R.V. Pound, Resonance absorption by nuclear magnetic moments in a solid, Phys. Rev. 69 (1946) 37–38.
[2] F. Bloch, Nuclear induction, Phys. Rev. 70 (1946) 460–474.
[3] F. Bloch, W.W. Hansen, M. Packard, The nuclear induction experiment, Phys. Rev. 70 (1946) 474–485.
[4] H.C. Torrey, Transient nutations in nuclear magnetic resonance, Phys. Rev. 76 (1949) 1059–1068.
[5] E. Hahn, Spin echoes, Phys. Rev. 80 (1950) 580–594.
[6] R.R. Ernst, Magnetic resonance with stochastic excitation, J. Magn. Reson. 3 (1970) 10–27.
[7] R. Kaiser, Coherent spectrometry with noise signals, J. Magn. Reson. 3 (1970) 28–43.
[8] R.R. Ernst, W.A. Anderson, Application of Fourier transform spectroscopy to magnetic resonance, Rev. Sci. Instrum. 37 (1966) 93–102.
[9] R.R. Ernst, G. Bodenhausen, A. Wokaun, Principles of Nuclear Magnetic Resonance in One and Two Dimensions, Clarendon Press, Oxford, 1997.
[10] H. Nilgens, M. Thelen, J. Paff, P. Blumler, B. Blumich, Hadamard NMR imaging with slice selection, Magn. Reson. Imaging 14 (1996) 857–861.
[11] A.J. Fagan, G.R. Davies, J.M. Hutchison, F.P. Glasser, D.J. Lurie, Development of a 3-D, multi-nuclear continuous wave NMR imaging system, J. Magn. Reson. 176 (2005) 140–150.
[12] M. Garwood, L. DelaBarre, The return of the frequency sweep: designing adiabatic pulses for contemporary NMR, J. Magn. Reson. 153 (2001) 155–177.
[13] J. Dadok, R.F. Sprecher, Correlation NMR spectroscopy, J. Magn. Reson. 13 (1974) 243–248.
[14] R.K. Gupta, J.A. Ferretti, E.D. Becker, Rapid scan Fourier transform NMR spectroscopy, J. Magn. Reson. 13 (1974) 275–290.
[15] R. Ouwerkerk, R.G. Weiss, P.A. Bottomley, Measuring human cardiac tissue sodium concentrations using surface coils, adiabatic excitation, and twisted projection imaging with minimal T_2 losses, J. Magn. Reson. Imaging 21 (2005) 546–555.
[16] D.S. Fieno, R.J. Kim, W.G. Rehwald, R.M. Judd, Physiological basis for potassium (^{39}K) magnetic resonance imaging of the heart, Circ. Res. 84 (1999) 913–920.
[17] P. Bendel, Biomedical applications of ^{10}B and ^{11}B NMR, NMR Biomed. 18 (2005) 74–82.
[18] M.S. Silver, R.I. Joseph, D.I. Hoult, Selective spin inversion in nuclear magnetic resonance and coherent optics through an exact solution of the Bloch–Riccati equation, Phys. Rev. A 31 (1985) 2753–2755.
[19] A. Tannus, M. Garwood, Improved performance of frequency-swept pulses using offset-independent adiabaticity, J. Magn. Reson. A 120 (1996) 133–137.
[20] Z.H. Cho, J.P. Jones, M. Singh, Foundations of Medical Imaging, Wiley, New York, 1993.
[21] J.I. Jackson, C.H. Meyer, D.G. Nishimura, A. Macovski, Selection of a convolution function for Fourier inversion using gridding, IEEE Trans. Med. Imaging 10 (1991) 473–478.
[22] B.A. Jacobsohn, R.K. Wangsness, Shapes of nuclear induction signals, Phys. Rev. 73 (1948) 942–946.
[23] R.R. Ernst, Sensitivity enhancement in magnetic resonance, Adv. Magn. Reson. 2 (1966) 1–135.
[24] J. Pipe, Spatial encoding and reconstruction in MRI with quadratic phase profiles, Magn. Reson. Med. 33 (1995) 24–33.

[25] J.-Y. Park, L. DelaBarre, M. Garwood, Improved gradient-echo 3D MRI using pseudo-echoes created by frequency-swept pulse, Magn. Reson. Med. 55 (2006) 848–857.
[26] I.J. Lowe, R.E. Norberg, Free-induction decays in solids, Phys. Rev. 107 (1957) 46–61.
[27] D. Shaw, Fourier Transform NMR Spectroscopy, Elsevier, Amsterdam, New York, 1984.
[28] J.A. Ferretti, R.R. Ernst, Interference effects in NMR correlation spectroscopy of coupled spin systems, J. Chem. Phys. 65 (1976) 4283–4293.
[29] S. Hafner, Fast imaging in liquids and solids with the back-projection low angle shot (BLAST) technique, Magn. Reson. Imaging 12 (1994) 1047–1051.
[30] D.P. Madio, I.J. Lowe, Ultra-fast imaging using low flip angles and fids, Magn. Reson. Med. 34 (1995) 525–529.
[31] C.J. Bergin, J.M. Pauly, A. Macovski, Lung parenchyma: Projection reconstruction MR imaging, Radiology 179 (1991) 777–781.
[32] M.D. Robson, P.D. Gatehouse, M. Bydder, G.M. Bydder, Magnetic resonance: an introduction to ultrashort TE (UTE) imaging, J. Comput. Assist. Tomogr. 27 (2003) 825–846.
[33] H. Nilgens, B. Blumich, Stochastic spectroscopic imaging, in: D.N. Rutledge (Ed.), Signal Treatment and Signal Analysis in NMR, Elsevier, Amsterdam, 1996, pp. 489–512.
[34] O. Hirsch, G. Scheler, C. Jager, Spectrometer for stochastic solid-state nuclear magnetic resonance spectroscopy, Rev. Sci. Instrum. 72 (2001) 1734–1741.